The impact of crystal morphology on the thermal responses of ultrasonically-excited energetic materials

J. K. Miller,[1,2,3,4] J. O. Mares,[2,5] I. E. Gunduz,[1,2] S. F. Son,[1,2,5] and J. F. Rhoads[1,3,4]
[1]*School of Mechanical Engineering, Purdue University, West Lafayette, Indiana 47907, USA*
[2]*Maurice J. Zucrow Laboratories, Purdue University, West Lafayette, Indiana 47907, USA*
[3]*Ray W. Herrick Laboratories, Purdue University, West Lafayette, Indiana 47907, USA*
[4]*Birck Nanotechnology Center, Purdue University, West Lafayette, Indiana 47907, USA*
[5]*School of Aeronautics and Astronautics, Purdue University, West Lafayette, Indiana 47907, USA*

(Received 2 November 2015; accepted 30 December 2015; published online 13 January 2016)

The ability to detect explosive materials may be significantly enhanced with local increases in vapor pressure caused by an elevation of the materials' temperature. Recently, ultrasonic excitation has been shown to generate heat within plastic-bonded energetic materials. To investigate the impact of crystal morphology on this heating, samples of elastic binder are implanted with single ammonium perchlorate crystals of two distinct shape groups. Contact piezoelectric transducers are then used to excite the samples at ultrasonic frequencies. The thermal responses of the crystals are recorded using infrared thermography, and the rate of heating is estimated. Surface temperature increases up to 15 °C are found to arise after 2 s of excitation, with much higher heating levels expected near the inclusions themselves as demonstrated by the chemical decomposition of some crystals under favorable excitation conditions. The rates of heat generation are compared to various crystal morphology features through 2D estimates of length scale, perimeter and irregularity. It is observed that crystals grown in the lab, featuring sharp geometric facets, exhibit a higher probability of significant heat generation than inclusions with more spherical shapes. However, no statistical link is found between the rates of heat generation and the crystal morphology in those samples that do generate significant heating, likely because variations in surface roughness cannot be entirely eliminated during experimentation. It is hoped that this study will lead to a better understanding of the nature of heat generation in energetic materials from ultrasonic sources. © *2016 AIP Publishing LLC*. [http://dx.doi.org/10.1063/1.4939812]

I. INTRODUCTION

The preferential generation of heat within energetic materials can be exploited in a variety of explosives detection and defeat applications, as well as in the development of a more fundamental understanding of mechanical energy localization in solids. As noted by Moore[1] and Ostmark,[2] the strong correlation between material temperature and vapor pressure for many common explosive compositions implies that an elevation of internal temperature can lead to increased concentrations of detectable vapors in the surrounding media. As such, understanding and exploiting heat generation within these materials could greatly assist current trace vapor detection technologies. In addition, temperature elevation above some critical threshold often leads to internal phase changes and eventually ignition within energetic materials, resulting in a possible explosives defeat mechanism. Accordingly, methods to generate heat within explosives, particularly from standoff sources, are highly beneficial in defense against security threats such as improvised explosive devices (IEDs).

To date, the generation of heat in energetic materials in response to mechanical excitation has been explored across two broad frequency regimes. First, a low-frequency range (10 s–100 s of Hz) has been explored wherein high-power excitation has led to the decomposition of ammonium perchlorate (AP) samples,[3] a phenomenon linked with dislocation and frictional heating effects. In mock composite energetic materials, which typically consist of crystals held within an elastic binder material, a viscoelastic type of heating has been observed.[4,5] This behavior can be explained by the phase differences between the stress and strain fields present within the material, which are attributable to hysteric damping. Heating akin to this is most strongly generated at the foci of the principle vibration modes of the structure as a whole. In the second, ultrasonic, frequency range, a viscoelastic heating effect is commonly cited,[6] wherein there exists significant correlation between surface temperature and surface velocity patterns within select frequency regimes. A second heating effect, centered upon embedded crystals, has also been observed in prior work by the authors[6,7] and others[8,9] at select ultrasonic frequencies. The latter effect exhibited little correlation between surface velocity and temperature patterns though, suggesting crystal-level frictional or stress concentration effects. In certain cases, through this type of heating, individual energetic crystals were led to chemical decomposition. From a key prior work,[6] it was postulated that the crystal morphology of the inclusions was of vital importance to the heat generation phenomenon; however, no quantitative link was established.

Prior works have detailed the effect of crystal shape on the sensitivity of explosives to both shock and impact. Loginov *et al.*[10] found that PETN crystals of an irregular shape were more sensitive to vibration than crystals that

were more rounded. In a study on the influence of crystal morphology on the shock sensitivity of detonation of RDX crystals,[11] evidence is provided that "angular" crystals on the size range of 100 to 300 μm are more sensitive to shock than "rounded" inclusions. Surface level "dimpling" on a 10–30 μm scale was noted as important. An additional study[12] suggested that additives may be effectively used to produce more spherical inclusions and thus reduce the shock sensitivity. Van der Steen *et al.*[13] noted similar trends to those outlined above in drop weight sensitivity, and an effective doubling of the run to detonation with the use of regularly shaped particles. Hudson *et al.*[14] suggested that the "smoothness" of RDX crystals significantly decreased the viscosity of the composite, which compared well with shock sensitivity data. Finally, Lecume *et al.*[15] presented tapping mode AFM measurements of RDX crystals and suggested that intergranular heterogeneities corresponded with shock sensitivity. While the mechanisms behind hot spot generation in shock or impact loading within the described studies may be distinct from those of the comparatively low-power mechanical excitation utilized in the present work, it is interesting to note the often repeated trend of sensitivity with crystal morphology.

To date, there has been no corresponding study on the effects of crystal morphology variation on heating caused by ultrasonic mechanical excitation. The objective of the current work is to quantify the rates of heating of two distinct morphological sets of AP crystals embedded in a binder. In this case, single inclusions are subjected to incident mechanical excitation near 215 kHz (near the center frequency of the utilized transducer). Two-dimensional image analysis techniques are then used to quantify the crystal morphology, and by fitting the surface temperature responses to an analytical model, the heat generation rates are predicted and compared.

II. SAMPLE PREPARATION

A. Crystal selection

To quantify the effects of crystal morphology on the heating phenomenon, two distinct morphologies of AP crystals were prepared. Highly spherical crystals of AP were selected directly from a lot received from the supplier (Firefox Enterprises, Inc.). These crystals were first selected by their ability to roll on a low friction surface and were then reviewed by microscopy to exclude those crystals with significant internal voids or evident crystal fractures. A range of crystal length scales from 600 to 1000 μm were selected. For the second set, AP crystals were dissolved in acetone and recrystallized into intentionally irregular crystalline forms through controlled evaporation over the course of several days. These crystals were again reviewed by microscopy to ensure a similar length scale to the first set. Seventeen crystals of each type were selected. Figure 1 presents representative images of the two crystal types examined, highlighting the obvious visual differences between them. It is important to note that while crystals of the spherical set were selected for a lack of significant sharp features, clear asperities were evident in the microscope images. However, these features are on the whole less severe and relatively smaller than those of the recrystallized set, as shown in Figure 1.

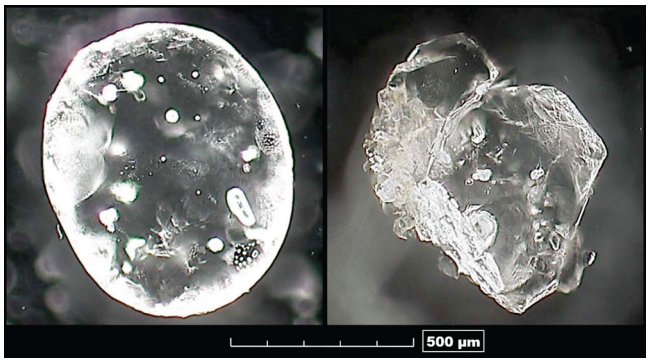

FIG. 1. Sample microscope images of representative (left) "spherical" and (right) "recrystallized" AP crystals.

B. Binder encapsulation

To encapsulate each crystal in binder, multiple curing steps were necessary. First, base layers of Sylgard 184 with thicknesses of 1 ± 0.2 mm were produced inside Petri dishes and allowed to cure completely at 65 °C. A secondary layer of uncured Sylgard was then added, and the crystals of interest were placed inside the uncured elastomer resting upon the 1 mm base layer underneath. This two-step curing process allowed for samples with a consistent distance of 1 mm between the inclusion and the "top" surface. The composite systems were then cured at 65 °C. Next, centered upon each crystal, rectangular samples of approximately 9×6.7 mm were cut out by hand. Each cutout was then placed into a mold which was then filled with a final layer of uncured Sylgard. A plunger was used to restrict the final sample outer dimensions to $9 \times 6.7 \times 4$ mm. Before each curing step, the Sylgard elastomer was degassed with a vacuum pump for a minimum of 10 min to eliminate internal voids due to gas entrapment. After the final layers of binder were fully cured, high-resolution optical photographs were taken for each sample via a Hirox KH-8700 digital microscope. Seventeen samples were created for each set of crystal shape, and five "blank" samples were created without a crystal inclusion as a control group.

III. EXCITATION AND SENSING

A. Electronic excitation

Steiner & Martins, Inc., SMD10T2R111 ultrasonic piezoelectric transducers were epoxied to the "bottom" side of each sample (i.e., the side further from the 1 mm base layer and embedded crystal) with Devcon 5 minute epoxy and cured at 65 °C overnight. Electrical excitation was provided to the ultrasonic transducers via an Agilent N9310A RF signal generator in concert with a Mini-Circuits LZY-22+ broadband amplifier. A Tektronix DPO 4043 oscilloscope was used to monitor the supply signal. Each sample was excited with a sine wave input across 100 logarithmically spaced points between 200 and 230 kHz. This frequency range was chosen due to its exhibition of crystal-based

heating in a prior work,[6] and is coincident with the center frequency of the transducers. Two seconds of electrical power was supplied at each frequency, with an input electrical power of 6.3 W.

B. Thermal measurement

The transient surface temperature of each sample in response to the excitation as described above was recorded via a FLIR A325sc infrared thermographic camera. This camera has a maximum sampling rate of 30 Hz, a temperature sensitivity of 0.07 °C at 30 °C, and a temperature accuracy of ±2 °C or ±2% of the reading. To ensure a constant infrared emissivity and to reduce the effects of background reflections on the measurements, the surface of each sample was coated in carbon black. Through a LabVIEW controller, the samples were cooled after every frequency step until mean and standard deviation thresholds were met, in order to ensure comparable starting conditions for each trial. In Figure 2, a block diagram of the excitation and measurement pathways is presented.

IV. RESULTS

A. Sample characterization

Analysis of the high-magnification photographs of each crystal permitted the estimation of quantifiable differences between the two sets through image analysis techniques. Utilizing a combination of the GNU Image Manipulation Program (GIMP) and ImageJ, a freely available crystal analysis software, the outlines of each crystal were determined through the application of numerous binary intensity thresholds. In situations where this approach produced unsatisfactory results, crystal boundaries were selected by hand, guided by a careful consideration of slight variations in image intensity. A sample crystal image and its final established boundary are presented in Figure 3, to highlight a representative result.

With the crystal boundaries determined, two-dimensional imaging processing techniques within ImageJ were used to quantify crystal perimeter, area, circularity, etc. Circularity comprises a comparison of a shape to a perfect circle, with a circularity of one representing an exact circle and zero representing a theoretical entirely irregular shape. The metric, first described by Cox,[16] is defined mathematically by

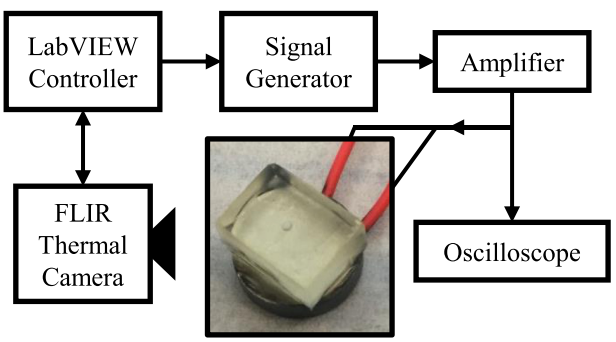

FIG. 2. Block diagram of excitation and measurement pathways used for the heat generation experiments.

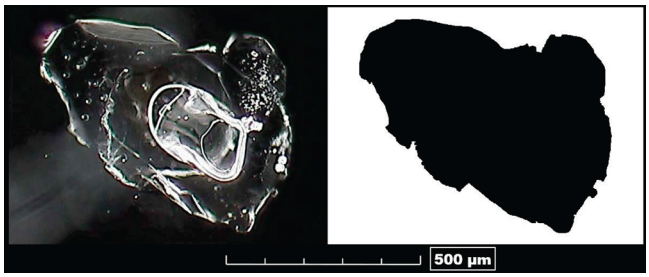

FIG. 3. Comparison between (left) optical image and (right) established crystal boundary for a representative recrystallized AP sample.

$$Circularity = 4\pi \frac{Area}{Perimeter^2}. \quad (1)$$

For the purposes of this paper, a "mean unrolled diameter" metric is used as a measure of length scale for all crystals. This measurement is taken as twice the average distance from the area centroid of each crystal to all points along the outer boundary. In the case of concave features, the multiple possible measurements are averaged. It is acknowledged that, because a single two-dimensional image was used to estimate these metrics, there is some degree of uncertainty in all measurements especially in those of the irregular set. The circularity and length scale spread of both sets of crystals is presented in Figure 4. As evident from the figure, there is a clear circularity difference between the two sets, quantifying the visually evident differences in crystal morphology.

B. Thermal modeling

To compare the aforementioned crystal morphology metrics with thermal data, the recorded thermographic camera data files were processed. First, the recorded spatial temperature data were sampled at a point directly above the crystal into one-dimensional temperature vs. time profiles for each excitation frequency. For each sample, the temperature profile exhibiting the maximum temperature increase after 2 s was chosen for analysis. Some variation in peak thermal response frequency was observed, an expected effect given

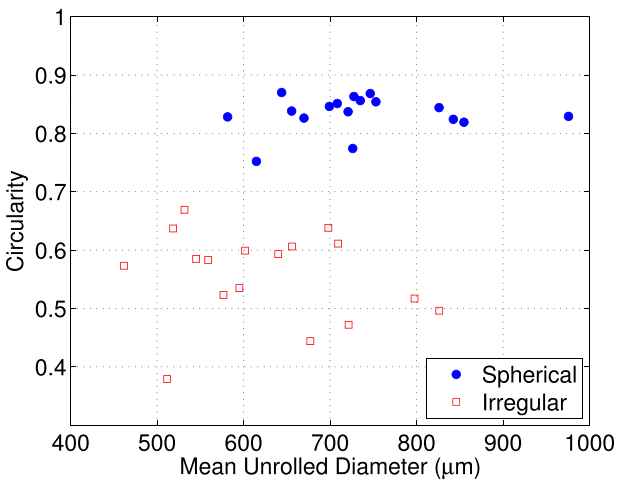

FIG. 4. Circularity vs. mean unrolled diameter for both spherical and recrystallized sample sets. Note the clear separation in circularity, and the broad spread of length scale (as expressed by mean unrolled diameter).

the natural slight variations in size and shape between transducers. Figure 5 presents the maximum temperature at the surface after 2 s of electrical excitation for all of the samples. Note that the temperature increase at the crystal itself is expected to be significantly greater than that measured at the surface.

Each thermal response was fit (via a least-squares approach) to a one-dimensional model for the transient temperature profile of a point source in a semi-infinite conductive medium. From the work of Carslaw and Jaeger,[17] a point source of heat generation rate q buried at a distance d from an insulated boundary will produce a temperature response given by

$$T_s(t) = \frac{q}{2\pi kd}\operatorname{erfc}\left(\frac{d}{\sqrt{4\alpha t}}\right), \tag{2}$$

where T_s is the increase in surface temperature, k and α are the thermal conductivity and diffusivity of the medium, respectively, erfc is the complimentary error function, and t is the time elapsed from the initial heat generation. Due to the nature of this analytical solution, and most notably its reliance on the complementary error function, one can expect there to be some uncertainty in the prediction of input parameters. A broad range of input parameters may be used to produce very similar temperature profiles, which in the presence of camera noise may cause systematic estimation errors. To address this concern, the camera noise was quantified through a reference recording of a constant temperature object. The noise levels measured from this test were predicted to affect source strength estimates by approximately 2%. In addition, the heating behavior is expected to occur at an isolated "hot spot" at an unknown location on the perimeter of the finite-sized crystal, and the heterogeneous thermal properties of the surrounding crystal and binder would affect the relevance of the simplified analytical solution. However, a finite element simulation of the effects of a variety of heat sources (including simulated point sources at the top, bottom, and sides of the crystal, as well as distributed sources) on the heat source strength estimation was performed, and suggested a maximum error of approximately 10% of the physical values. The fitted d parameters were all checked for relevance to the physical distances from each crystal to the surface, and the fitted q values were compared between samples as an estimate of the susceptibility of each to this heating phenomenon.

C. Heating results

The estimated rates of heat generation for the three sets of samples are presented in Figure 6. The five blank samples exhibited no significant heating, suggesting that the observed effects may be attributed to the included crystals. Between the two remaining sets, the irregular crystals produced more heat on average than their spherical counterparts. On closer inspection, the spherical crystals may be separated into two distinct groups: one with very low heat generation and the other largely indistinguishable from the irregular set. As only spherical crystals exhibit the very low heating phenomenon, it is posited that below some irregularity threshold, no significant heat may be generated. However, it is noted that the very low rates of estimated heat generation still outpace the blank samples. Therefore, it is proposed that some form of weak viscoelastic heating takes place in all samples with included crystals, with heat generated by a hysteretic response in the elastic binder as it deforms near the crystal.

The non-normal distribution of the spherical set does not allow for a direct comparison of the mean values between sets. Due to this, the probability for a "go" condition (>50 mW) was tested to define a statistically significant difference between the irregular and spherical samples. The probability for significant heating was 100% and 47.1% for the irregular and spherical samples, respectively, resulting in a p-value of less than 0.001 using the condition of a large sample test of proportions. Thus, there exists a significant difference in the probability of significant heating between the irregular and spherical samples. Due to this, the

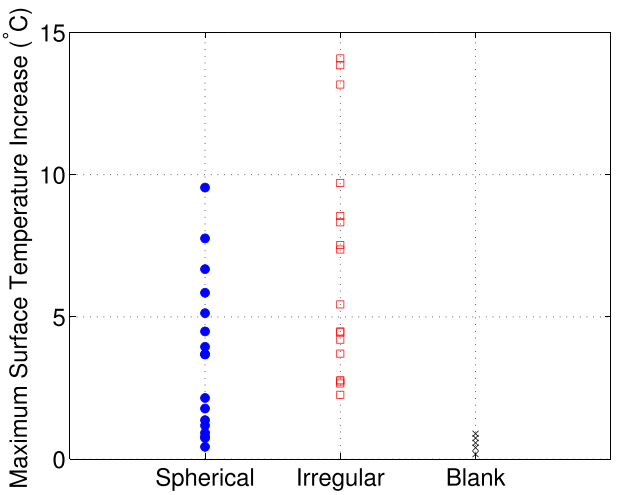

FIG. 5. Maximum increases in surface temperature after 2 s of electrical excitation for all three sample sets. Note the extremely low temperature responses noted for all of the blank samples, and the bimodal distribution of response in the spherical set.

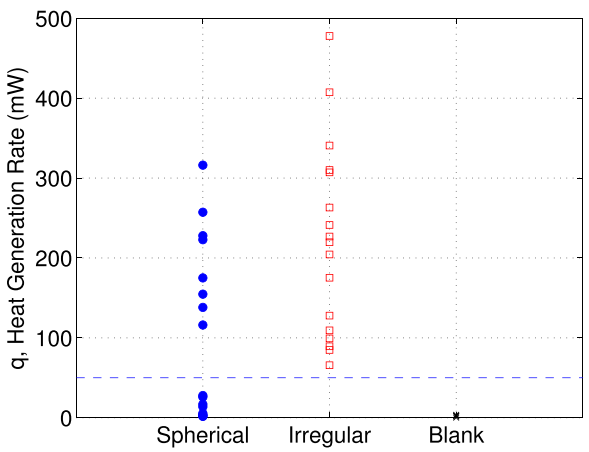

FIG. 6. Heat generation rates for all three sample sets, with a 50 mW threshold indicated. Note the high mean heat generation rate exhibited by the recrystallized samples, the binary nature of heat generation within the spherical set, and the very low levels of heat generation from the five blank samples.

mechanism of heating in the "go" samples is believed by the authors to be associated with the crystal morphology. This effect may be caused by a frictional effect at a favorable crystal asperity, or due to the same viscoelastic heating proposed in the "no go" samples exacerbated by the significant stress concentrations to be expected at these asperities. "Go" samples within the spherical set may contain rough features on a smaller scale than that measured in the present work.

That being said, there was little direct correlation between samples exhibiting strong heating and those with comparatively high circularity as perhaps expected. The heat generation of each set as a function of circularity is presented in Figure 7. Statistical analysis on the relationship between heat generation and circularity within samples estimated to heat at a rate greater than 50 mW resulted in a p-value of 0.863, indicating virtually no dependence of heating rates on the crystal morphology of the samples. These results indicate that crystal morphology only influences the probability for significant heating, but that once significant heating is observed, there is no apparent relationship between heat generation and morphology. This may be due to the previously described uncertainty associated with two-dimensional image analysis or to a heating mechanism caused by interactions on a smaller scale than that which was evaluated.

The heat generation rates of both sets of crystal inclusions is compared with the length scale, here approximated as the mean unrolled diameter, in Figure 8. For all crystals estimated to generate heat at a rate above 50 mW, there is no significant dependence on length scale, with a p-value of 0.239. This result is of interest given that a study conducted by Loginov[10] found that an increase in sensitivity due to vibration was associated with larger crystals. However, that result was found in multiple crystals in contact without binder and may not be applicable in these single-crystal systems. Finally, the effect of perimeter on the heat generation rates of those samples which were estimated to be above 50 mW yielded a p-value of 0.218, which does not indicate a significant relationship.

The aforementioned results indicate that, while surface morphology affects the probability of a crystal to develop

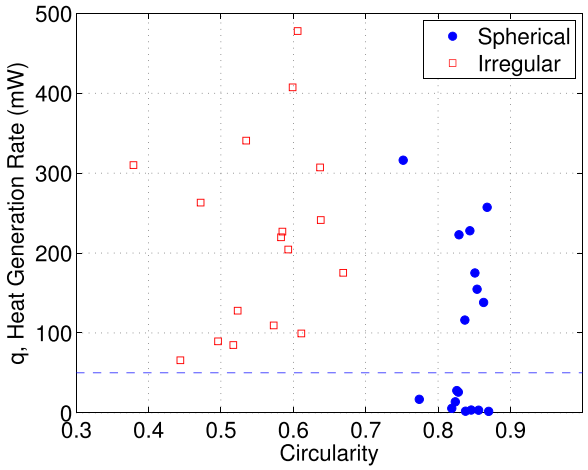

FIG. 7. Heat generation rates vs. circularity for all of the samples, with a 50 mW threshold indicated. No significant trends are present.

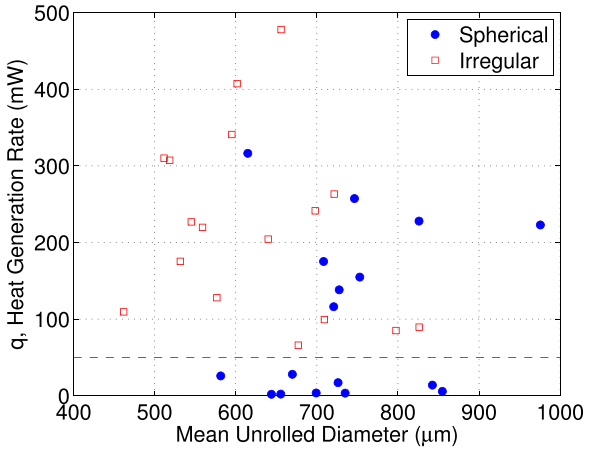

FIG. 8. Heat generation rates vs. mean unrolled diameter for all of the samples, with a 50 mW threshold indicated. Note the slight negative correlation with length scale for all samples above the 50 mW threshold.

significant heat in response to ultrasonic excitation, the rate of that heating does not correlate with any of the measured quantities. This may suggest that hot spots develop at discrete favorable surface asperities and that an increase in surface area or irregularity does not contribute to the heating rate of any single hot spot. If numerous hot spots were to occur at the crystal/binder interface, results should have indicated a relationship between surface area, crystal irregularity, and heat generation.

In addition to the reported analysis, a higher susceptibility to significant heating was confirmed through the use of an increased electrical input power level. Three out of five recrystallized AP samples were led to energetic decomposition at an input electrical power level of 10 W, which in the same study caused only one out of seven unmodified AP crystals to decompose. This decomposition is induced through the onset of a significant temperature excursion within the material, indicative of a very strong local heating effect. For the work presented herein, the input power level was reduced to 6.3 W, which did not induce decomposition in any sample. Additional work should examine the heating phenomena at higher input powers.

V. CONCLUSIONS

The thermal responses of embedded spherical and irregular AP crystals under high-frequency mechanical excitation have been presented. The transient temperature profile of each crystal was fit to an analytical solution for a point heat source in a semi-infinite medium in order to estimate the rate of heat generation. A statistically significant difference has been identified in the probability of significant heat generation between sets of distinct crystal morphology. Two mechanisms for heating are proposed: a weak heating associated with viscoelastic heating of the surrounding binder and a stronger, surface asperity-based effect. This stronger heating may be the same viscoelastic heating exacerbated by stress concentrations or a secondary, frictional effect. However, neither the effects of irregularity, as expressed through circularity, nor length scale or perimeter measurements presented significant trends compared with the heating rates of

individual crystals. In light of these observations, it is posited that a low number of "hot spots" are formed around the perimeter of each crystal due to discrete surface asperities, and that the severity of the irregularity itself is not intrinsically important to the thermal response generated within. That is to say, while a highly irregular crystal has a greater probability of generating the stronger type of heating, it does not offer a quantifiable increase in the rate of heat generation itself. It is interesting to compare this observation with prior works in shock and impact excitation, which suggest in all cases that more irregular crystals lead to more sensitive materials. While the mechanisms of hot spot generation may very well be quite different between the present work and these studies, the susceptibility of highly irregular crystals to strong, localized thermal responses seems to be a common effect. Future studies will explore the effects of crystal size, binder adhesion, and multiple crystals on this heating phenomenon.

ACKNOWLEDGMENTS

This research was supported by the U.S. Office of Naval Research under the Multidisciplinary University Research Initiative on "Sound and Electromagnetic Interacting Waves" through Grant No. N00014-10-1-0958 and under the Basic Research Challenge on "Chemical Decomposition in High Energy Density Materials Induced by Coupled Acoustic Electromagnetic Energy Insult" through Grant No. N00014-11-1-0466. J.O.M. also wishes to acknowledge the National Science Graduate Research Fellowship Program under Grant No. DGE-1333468.

[1]D. S. Moore, Rev. Sci. Instrum. **75**, 2499 (2004).
[2]H. Ostmark, S. Wallin, and H. G. Ang, Propellants, Explos., Pyrotech. **37**, 12 (2012).
[3]N. Loginov, S. Muratov, and V. Epifanov, Combust., Explos. Shock Waves **25**, 58 (1989).
[4]J. K. Miller, D. C. Woods, and J. F. Rhoads, J. Appl. Phys. **116**, 244904 (2014).
[5]D. C. Woods, J. K. Miller, and J. F. Rhoads, J. Vib. Acoust. **137**, 054502 (2015).
[6]J. O. Mares, J. K. Miller, I. E. Gunduz, J. F. Rhoads, and S. F. Son, J. Appl. Phys. **116**, 204902 (2014).
[7]J. O. Mares, J. K. Miller, N. D. Sharp, D. S. Moore, D. E. Adams, L. J. Groven, J. F. Rhoads, and S. F. Son, J. Appl. Phys. **113**, 084904 (2013).
[8]M.-W. Chen, S. You, K. S. Suslick, and D. D. Dlott, Rev. Sci. Instrum. **85**, 023705 (2014).
[9]S. You, M.-W. Chen, D. D. Dlott, and K. S. Suslick, Nat. Commun. **6**, 6581 (2015).
[10]N. Loginov, Combust., Explos. Shock Waves **45**, 64 (2009).
[11]H. Czerski and W. G. Proud, J. Appl. Phys. **102**, 113515 (2007).
[12]D.-X. Wang, S.-S. Chen, Y.-Y. Li, J.-Y. Yang, T.-Y. Wei, and S.-H. Jin, J. Energ. Mater. **32**, 184 (2014).
[13]A. C. Van der Steen, H. J. Verbeek, and J. J. Meulenbrugge, in Proceedings of the 9th Symposium on Detonation, 1989, p. 83.
[14]R. J. Hudson, M. Moniruzzaman, and P. P. Gill, Propellants, Explos., Pyrotech. **40**, 233 (2015).
[15]S. Lecume, C. Spyckerelle, and F. Sommer, AIP Conf. Proc. **706**, 997 (2004).
[16]E. Cox, J. Paleontol. **1**, 179 (1927).
[17]H. Carslaw and J. Jaeger, *Conduction of Heat in Solids* (Clareden Press, 1959).